

# **3rd Warsaw School of Statistical Physics**

Kazimierz Dolny, Poland

## DENSITY FUNCTIONAL THEORY FOR INHOMOGENEOUS FLUIDS II (FREEZING, DYNAMICS, LIQUID CRYSTALS)

**Hartmut Löwen**

Heinrich-Heine University Düsseldorf, Germany

27 June - 3 July 2009

# Outline

<b>1</b>	<b>Density functional theory of freezing: spheres</b>	<b>2</b>
1.1	Phenomenological results . . . . .	2
1.2	Independent treatment of the different phases . . . . .	3
1.3	Unifying Microscopic theories . . . . .	4
1.4	Phase diagrams of simple potentials . . . . .	5
1.5	Density Functional Theory (DFT) . . . . .	9
<b>2</b>	<b>Brownian Dynamics and dynamical density functional theory</b>	<b>15</b>
2.1	Brownian dynamics (BD) . . . . .	15
2.2	Dynamical density functional theory (DDFT) . . . . .	18
2.3	Hydrodynamic interactions . . . . .	22
<b>3</b>	<b>Density functional theory for rod-like particles</b>	<b>24</b>
3.1	Statistical mechanics of rod-like particles . . . . .	24
3.2	Simple models . . . . .	28
3.3	Brownian dynamics of rod-like particles . . . . .	32
<b>4</b>	<b>Conclusions</b>	<b>34</b>

**Abstract:**

These lectures form the second part of classical density functional theory (DFT) following the lectures of R. Evans (part I).

First, after a brief reminder of equilibrium density functional theory, DFT is applied to the *freezing* transition of liquids into crystalline lattices. First, spherical particles with radially symmetric pair potentials will be treated (like hard spheres, the classical one-component plasma or Gaussian-core particles).

Second, the DFT will be generalized towards Brownian *dynamics* in order to tackle nonequilibrium problems. After a general introduction to Brownian dynamics using the complementary Smoluchowski and Langevin pictures appropriate for the dynamics of colloidal suspensions, the dynamical density functional theory (DDFT) will be derived from the Smoluchowski equation. This will be done first for spherical particles (e.g. hard spheres or Gaussian-cores) without hydrodynamic interactions. Then we show how to incorporate hydrodynamic interactions between the colloidal particles into the DDFT framework.

Third orientational degrees of freedom (rod-like particles) will be considered as well. In the latter case, the stability of intermediate liquid crystalline phases (isotropic, nematic, smectic-A, plastic crystals etc) can be predicted. Finally, the corresponding dynamical extension of density functional theory towards orientational degrees of freedom is proposed.

This set of lectures will continue and supplement the preceding lectures of R. Evans on density functional theory. Here we shall focus on the freezing transition, on orientational degrees of freedom and on dynamical density functional theory for colloidal suspensions which are governed by Brownian dynamics.

# 1 Density functional theory of freezing: spheres

## 1.1 Phenomenological results

Experiments show that liquids freeze into periodic crystalline structures at low temperatures or high densities. In these states, the translational symmetry of the system is broken, i.e. the one-particle density  $\rho(\vec{r})$  is *inhomogeneous*. As freezing is ubiquitous and general, it is one of the most important phase transition in nature. The basic question is: when does it happen? Answering this question is one of the central tasks of statistical physics. A full microscopic theory is highly desirable which uses the interaction forces as an input and predicts the thermodynamic conditions for freezing as an output. Since freezing is a collective effect, this is a very demanding task.

Before turning to such a microscopic approach, let us first collect some *empirical facts* for freezing, as for more details and references, see [1, 2, 3, 4, 5, 6]. We shall also summarize known phase behaviour for simple model potentials gained by computer simulations.

### i) Lindemann-criterion of melting

If  $a = \rho^{-1/3}$  denotes a typical interparticle spacing (with the number density  $\rho$  being the number of particles per volume), then one can examine the root mean-square displacement  $u$  of a particle around a given crystalline lattice position  $\vec{R}_i$ ,  $i$  denoting a lattice site index, which is defined as

$$u = \sqrt{\langle (\vec{r}_i - \vec{R}_i)^2 \rangle} \quad (1)$$

This quantity can also be viewed as the spread of the inhomogeneous one-particle density  $\rho(\vec{r})$  around a lattice position, see Figure 1.

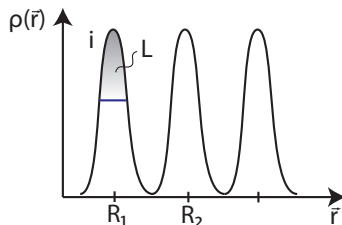


**Figure 1:** One-dimensional sketch of the inhomogeneous one-particle density  $\rho(\vec{r})$  in a crystalline solid with lattice points at  $\vec{R}_1$  and  $\vec{R}_2$ . The spread of the density peak is embodied in the Lindemann parameter  $L$ .

The Lindemann parameter  $L = u/a$  measures the fluctuations around the lattice positions in terms of the lattice constant. The traditional Lindemann rule of melting states that a solid melts if  $L \approx 0.1$ . Computer simulations have confirmed this phenomenological rule where the actual value of  $L$  at melting varies between 0.129 for hard spheres and 0.18 for the one-component plasma. But it is always roughly one order of magnitude smaller than the lattice constant itself.

ii) Hansen-Verlet rule of freezing

Different to the Lindemann rule, the Hansen-Verlet rule starts from the liquid side of the freezing transition and states that the freezing occurs if the amplitude of the first peak in the liquid structure factor  $S(k)$  (for a definition, see the lectures of R. Evans) exceeds 2.85, see Figure 2 for a schematic illustration. Originally found for Lennard-Jones systems, this rule has been confirmed also for other interactions like hard-sphere, plasma and Yukawa pair potentials. Without any notable exception a value of 2.5-3.0 was found near equilibrium freezing. However, the peak can be much higher in a metastable glassy state.

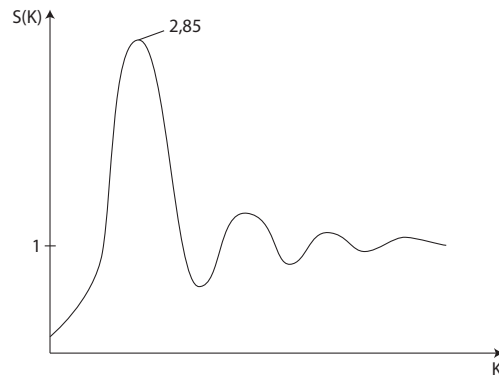


**Figure 2:** Sketch of a liquid structure factor  $S(k)$  versus  $k$  where the amplitude of the first peak is 2.85. According to the Hansen-Verlet rule, this is a liquid structure close to freezing.

## 1.2 Independent treatment of the different phases

The simplest theoretical approach is to construct different theories for the different thermodynamic states (solid and liquid). In particular the internal energy of the solid phase can be accessed by a simple lattice sum of the given pair potentials. In particular, different candidate lattices can be assumed at fixed averaged density, and the one with minimal potential energy will be the stable one for temperature  $T = 0$ . Finite temperature corrections based on a harmonic phonon-picture can be added on top of that resulting in a (Helmholtz) free energy  $F$  of the solid state.

Likewise the free energy of the liquid can be gained by using for instance liquid integral equation theories [7] where different closure schemes may be adopted.

Combined with the free energy of the solid, a Maxwell double-tangent construction for the isothermal free energy per particles versus density  $\rho$  leads to the coexisting liquid and solid densities  $\rho_\ell$  and  $\rho_s$ , see Figure 3. The double tangent ensures the equality of the chemical potential and the pressure in the two phases. If this is repeated for various temperature, the full phase diagram emerges. In three spatial dimensions, freezing is typically a first order transition with a considerable density jump  $\Delta\rho = \rho_s - \rho_\ell$ .

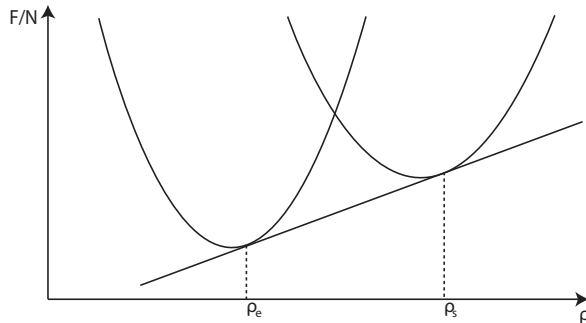


**Figure 3:** Sketch of the Maxwell double tangent construction to the free energy per particle in the liquid and solid phase resulting in the two coexistence densities  $\rho_\ell$  and  $\rho_s$ .

### 1.3 Unifying Microscopic theories

Both from a fundamental and esthetic point of view, a unifying theory which treats both the liquid and the solid phase on the same footing is desirable. In the past decades, there have been considerable advances in this field. In three spatial dimensions, classical density functional theory (DFT) (as described in the lectures of R. Evans) can be used to get a liquid-based description of the solid phase. Here the solid is viewed as a strongly inhomogeneous liquid with strong density peaks. Freezing in DFT is therefore a condensation of liquid density modes [5].

Conversely, in two spatial dimensions the Kosterlitz-Thouless approach is a solid-based approach which treats the liquid as a solid phase with an accumulation of defects.

In the following we shall focus on the three-dimensional freezing and on density functional theory. We emphasize that a unifying treatment is mandatory for the description of solid-liquid interface and phenomena like crystal nucleation and growth out of an undercooled melt where indeed a single theory for both phases is needed.

## 1.4 Phase diagrams of simple potentials

Let us first summarize some familiar phase diagrams for various model pairwise interactions. These were obtained mainly by "exact" computer simulation of a many-body system [8] and therefore provide "benchmark" data for a microscopic theory.

### a) hard spheres

The simplest nontrivial interaction potential is that for hard spheres of diameter  $\sigma$ . The potential reads

$$V(r) = \begin{cases} \infty, & r \leq \sigma \\ 0, & r > \sigma \end{cases} \quad (2)$$

The internal energy is completely ideal  $U = \frac{3}{2}Nk_B T$ , i.e. the averaged potential energy is zero. Hence Helmholtz free energy  $F = U - TS$  scales with  $k_B T$  alone (as  $k_B T$  is the only energy scale for hard spheres). Therefore, for hard spheres, the entire thermodynamic behaviour is governed by entropy alone. This becomes different for other interactions which possess an explicit energy scale. This is the main reason why hard spheres are the most important models for freezing. From computer simulations, the hard sphere phase diagram is shown in Figure 4. The only parameter is the density which is conveniently scaled in terms of a volume or packing fraction  $\eta = \pi\rho\sigma^3/6$ . The quantity  $\eta$  measures the ratio of the volume occupied by all spheres to the total available volume  $V$  of the system. For  $\eta \rightarrow 0$  an ideal gas is recovered, while maximal packing for hard spheres occurs for  $\eta = \eta_{cp} = 0.74$  corresponding to stacked layers of triangular crystals. In between, there is a first order freezing transition with coexisting packing fractions  $\eta_{ell} = 0.494$  and  $\eta_s = 0.545$ . The stable crystalline crystal is face-centred-cubic (fcc) which has an *ABC* stacking sequence. Interestingly, the freezing transition is driven by entropy. For  $\eta > \eta_s$  the solid state has a higher entropy than the fluid state clearly showing that entropy has nothing to do with structural order. More intuitively, a disordered fluid state at high densities implies jammed configurations, and much more configuration (i.e. higher entropy) is gained by taking as a reference configuration a solid and generating more configurations from slightly displaced particles (configurational entropy).

### b) plasma

The one-component plasma (OCP) with neutralizing background is defined by the pairwise Coulomb potential  $V(r) = V_0/r$ . By scaling the classical partition function, one can show that only the coupling parameter  $\Gamma = \frac{\sqrt[3]{\frac{4\pi\rho}{3}}V_0}{k_B T}$  determines the structure and phase behaviour. The freezing diagram of the OCP is summarized in Figure 5, there is isochoric freezing from the fluid into a body-centered-crystal (bcc) at  $\Gamma = 178$ .

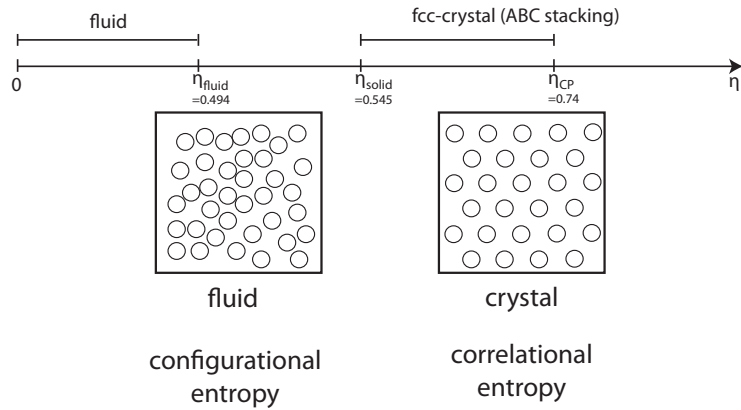


**Figure 4:** Hard sphere freezing diagram versus packing fraction  $\eta$ . The intuitive picture of freezing is also shown: at high densities a fluid state involves blocked configurations and more configurations are achieved by a periodic packing.

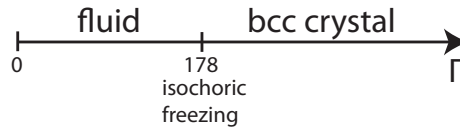


**Figure 5:** Isochoric freezing in the one-component plasma.

### c) soft spheres

Inverse power law potentials where  $V(r) = V_0(\sigma/r)^n$  interpolate between the plasma ( $n = 1$ ) and the hard sphere potential, formally obtained as  $n \rightarrow \infty$ . Depending on  $n$  either bcc or fcc crystals are stable.

### d) Yukawa-system

The Yukawa potential  $V(r) = V_0 \exp(-\kappa r)/r$  applies e.g. to charge-stabilized colloidal suspensions. Again  $\kappa$  interpolates between the OCP ( $\kappa = 0$ ) and the hard-sphere-limit  $\kappa \rightarrow \infty$ . The phase diagram depends only on  $\lambda = \kappa a$  ( $a = \rho^{-\frac{1}{3}}$ ) and  $\tilde{T} = \frac{k_B T}{V_0} \frac{e^\lambda}{\lambda}$  and involves a fluid, a bcc solid and an fcc solid with a triple point as sketched in Figure 6.

### e) Lennard-Jones-system

The Lennard-Jones potential, the traditional model for rare gases, is given by  $V(r) = 4\epsilon \left( \left(\frac{\sigma}{r}\right)^{12} - \left(\frac{\sigma}{r}\right)^6 \right)$  where  $\epsilon$  is the energy and  $\sigma$  is the length scale. This potential has a long-ranged attractive tail. Correspondingly it exhibits also a critical point separating a gas from a liquid and a triple point with gas-liquid-fcc solid coexistence. As a function of the two reduced parameters  $k_B T/\epsilon$  and  $\rho\sigma^3$  its phase diagram is sketched in Figure 7.



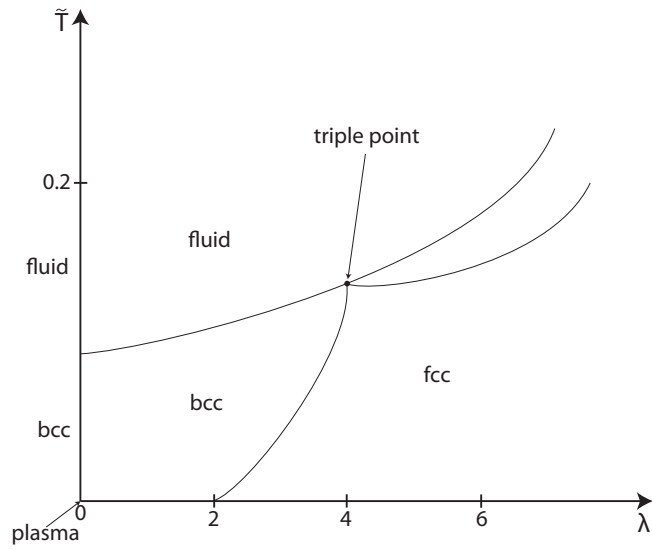


**Figure 6:** Sketch of the Yukawa phase diagram in the plane spanned by  $\lambda$  and  $\tilde{T}$ . The special case  $\lambda = 0$  is the one-component plasma.

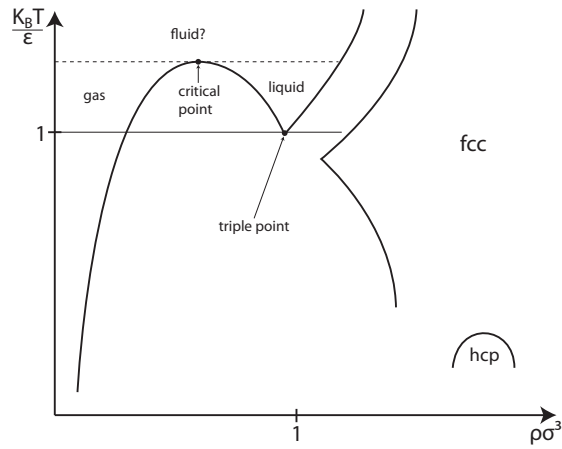


**Figure 7:** Sketch of the Lennard-Jones phase diagram in the plane spanned by reduced temperature  $k_B T/\epsilon$  and density  $\rho\sigma^3$ .

f) **sticky hard spheres**

Sticky hard spheres possess a square-well attraction and are reasonable models for proteins. Here

$$V(r) = \begin{cases} \infty & r \leq \sigma \\ -\epsilon & \sigma \leq r \leq \sigma(1 + \delta) \\ 0 & \text{elsewhere} \end{cases} \quad (3)$$

with a finite attraction range  $\delta\sigma$  and an attraction depth of  $-\epsilon$ . The scaled range  $\delta$  must be larger than about 0.25 in order to get a liquid-gas separation. For small  $\delta < 0.05$  there is a novel isostructural solid-solid-transition with a critical point [9], see Figure 8.

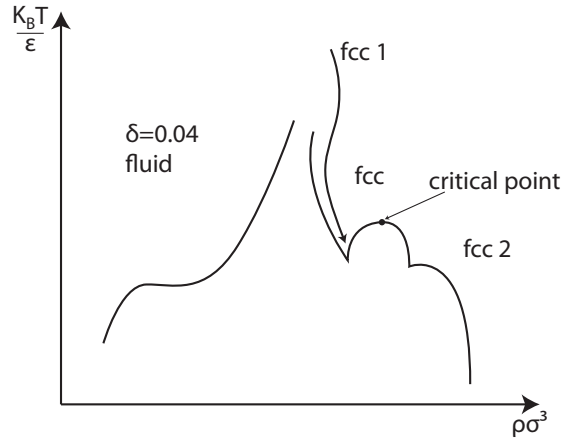


**Figure 8:** Sketch of the sticky hard sphere phase diagram in the plane spanned by reduced temperature  $k_B T / \epsilon$  and density  $\rho\sigma^3$ .

#### g) ultrasoft interactions

Soft (floppy) objects like polymer coils have effective interactions which are even softer than the plasma, therefore these interactions are called "ultrasoft" [10]. A log-Yukawa interaction has been proposed for star polymers. Here the interaction diverges at the origin only logarithmically with distance, i.e.  $V(r) \propto k_B T \ln(r/\sigma)$ . The phase behaviour [11] involves fluid, bcc and fcc solids as well as body-centered-orthogonal and diamond lattices and exhibits reentrance effects.

#### h) Penetrable interactions

One may even describe soft objects with pair potentials which are finite at the origin. Examples are Gaussian potentials which are a good model for linear polymer coils. The phase behaviour involves again the fluid, bcc-solid and fcc-solid phase with fluid reentrance [12]. Penetrable interactions with other shapes exhibit again also "exotic" solid phases and reentrance [13]. Finite potentials which have a negative Fourier transform exhibit cluster crystals [14] where a lattice points is occupied by more than one particle.

## Summary of 1.4:

- 1) Hard and “harsh” potential freeze into fcc lattices.
- 2) Soft repulsive potentials with an at least  $\frac{1}{r}$  singularity for  $r \searrow 0$  freeze into bcc lattices.
- 3) Ultrasoft  $v(r) \sim -\ln(\frac{r}{\sigma})$  and penetrable ( $V(r \searrow 0) = V(0) < \infty$ ) potentials show besides fcc and bcc structures, more open “exotic” lattices and reentrance effects.
- 4) If the Fouriertransform of  $V(r)$  has negative parts, a cluster crystal occurs.
- 5) Attractions lead to gas-liquid coexistence and isostructural solid-solid transition.

In conclusion, various shapes of the pairwise interaction potential can lead to a rich phase behaviour and there is the theoretical challenge to construct a microscopic approach in order to predict and reproduce this complex phase behaviour. As will be discussed in the sequel, classical density functional theory for inhomogeneous fluids does provide such an approach.

## 1.5 Density Functional Theory (DFT)

### a) Basics

The cornerstone of density functional theory (DFT) is an existence theorem combined with a basic variational principle [15]. In detail, there exists a unique grand-canonical free energy-density-functional  $\Omega(T, \mu, [\rho])$ , which gets minimal for the equilibrium density  $\rho_0(\vec{r})$  and then coincides with the real grandcanonical free energy, i.e.

$$\left. \frac{\delta\Omega(T, \mu, [\rho])}{\delta\rho(\vec{r})} \right|_{\rho(\vec{r})=\rho_0(\vec{r})} = 0. \quad (4)$$

In particular DFT is also valid for systems which are inhomogeneous on a microscopic scale. In principle, all fluctuations are included in an external potential which breaks all symmetries. For interacting systems in 3d, however,  $\Omega(T, \mu, [\rho])$  is not known.

Fortunately, there are few exceptions where the density functional is known exactly. First, for low density, the ideal-gas-limit is reached and the density functional can be constructed analytically (see below). Next leading orders for finite densities can be incorporated via a virial expansion which is quadratic in the densities. Conversely, in the high-density-limit, the mean-field approximation (see below) becomes asymptotically exact for penetrable potentials. Indeed this approximation also works surprisingly well for finite densities beyond overlap. Furthermore, the density functional is exactly known (as so-called Percus-functional) in one spatial dimension for the Tonks gas (hard rods on a line). However, the latter system does not exhibit freezing. Please note that the knowledge of a functional is much more than a bulk equation of state since it can be applied to any external potential  $V_{ext}(\vec{r})$ .

In principle, the application of DFT to freezing works as follows: First one has to choose an approximation. Then the density field is parameterized with variational parameters. In the homogeneous gas and liquid bulk phase one takes

$$\rho(\vec{r}) = \bar{\rho} \quad (5)$$

where  $\bar{\rho}$  is a variational parameter. On the other hand, for the solid, the Gaussian approximation of density peaks on the lattice positions is an excellent choice [16].

$$\rho(\vec{r}) = \left(\frac{\alpha}{\pi}\right)^{-3/2} \sum_n \exp\left(-\alpha(\vec{r} - \vec{R}_n)^2\right) \quad (6)$$

Here both the lattice structure and spacing as well as the width  $\alpha$  are variational parameters. Finally, for a given chemical potential  $\mu$  and temperature  $T$ , one has to minimize the functional  $\Omega(T, \mu, [\rho])$  with respect to all variational parameters. As a result one obtains the phase diagram in the  $\mu T$  plane.

The procedure itself is sketched close to the solid-liquid transition in Figures 9 and 10. A solid-liquid transition line in the  $\mu T$  plane is schematically shown in Figure 9 and we consider a path with fixed  $\mu$  and increasing  $T$  crossing the solid-liquid transition at  $\mu = \mu_{coex}$  and  $T = T_{coex}$ . Coexistence implies that temperature  $T$ , chemical potential  $\mu$  and pressure  $p$  are the same in both phases. Since in the bulk  $p = -\Omega/V$  ( $V$  denoting the system volume) coexistence means that at given  $\mu$  and  $T$ ,  $\Omega/V$  has two minima with equal depth. A contour plot of the density functional in the space of variational parameters is shown in Figure 10 for three different temperature on the path shown in Figure 9. The liquid minimum occurs at zero  $\alpha$  while the solid is characterized by a minimum at finite  $\alpha$ . The global minimum is the stable phase and at coexistence, the two minima have equal depth.

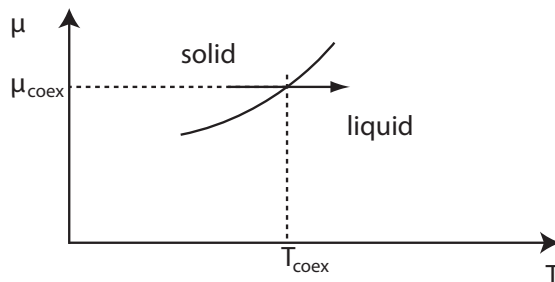


**Figure 9:** Solid-liquid coexistence line in the  $\mu T$  plane. The path along which three state points are discussed in Figure 10 is indicated.

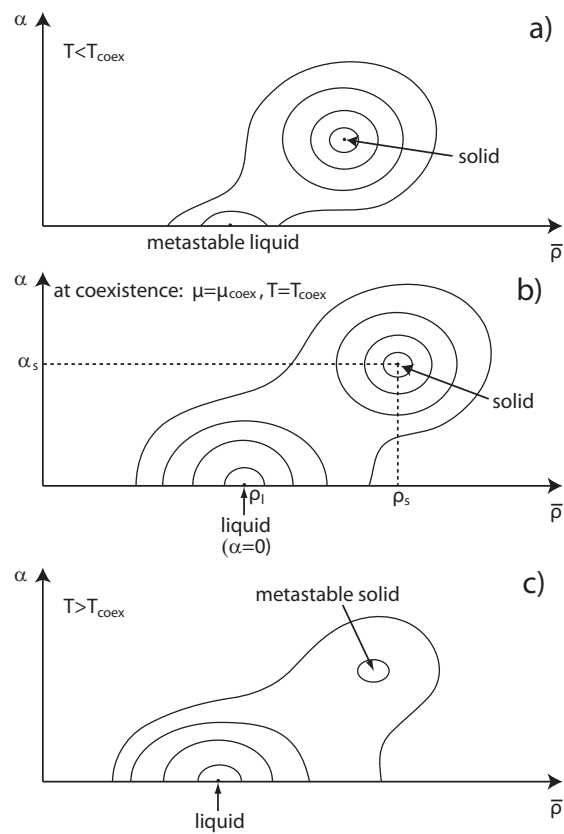


**Figure 10:** Contour plot of the grandcanonical free energy  $\Omega(T, \mu, \bar{\rho}, \alpha)$  for fixed  $T$  and  $\mu$  as a function of two variational parameters  $\alpha$  and the averaged density  $\bar{\rho}$ . The latter is given by the lattice constant in the solid phase. a) with a stable solid phase, b) at solid-liquid coexistence, c) with a stable liquid phase.

b) approximations for the density functional

Let us first recall the exact functional for the ideal gas where  $V(r) = 0$ . It reads as

$$\mathcal{F}_{\text{id}}(T, [\rho]) = k_B T \int d^3 r \rho(\vec{r}) [\ln(\rho(\vec{r})\Lambda^3) - 1] \quad (7)$$

and minimization

$$\left. \frac{\delta \mathcal{F}_{\text{id}}}{\delta \rho(\vec{r})} \right|_0 = k_B T \ln(\rho(\vec{r})\Lambda^3) + V_{\text{ext}}(\vec{r}) - \mu \quad (8)$$

leads to the generalized barometric law

$$\rho_0(\vec{r}) = \frac{1}{\Lambda^3} \exp\left(-\frac{V_{\text{ext}}(\vec{r}) - \mu}{k_B T}\right) \quad (9)$$

for the inhomogenous density. In the interacting case,  $V(r) \neq 0$ , one can split

$$\mathcal{F}(T, [\rho]) =: \mathcal{F}_{\text{id}}(T, [\rho]) + \mathcal{F}_{\text{exc}}(T, [\rho]) \quad (10)$$

which defines the excess free energy density functional  $\mathcal{F}_{\text{exc}}(T, [\rho])$ . Approximations work on different levels. In the *mean-field approximation*, we set

$$\mathcal{F}_{\text{exc}}(T, [\rho]) \approx \frac{1}{2} \int d^3 r \int d^3 r' V(|\vec{r} - \vec{r}'|) \rho(\vec{r}) \rho(\vec{r}') \quad (11)$$

In fact, the mean-field approximation (together with a correlational hole in the solid) yields freezing of the Gaussian potential [17] and is the correct starting point for cluster crystals for penetrable potentials [14].

The Ramakrishnan-Youssuf (RY) approximation is a perturbative treatment out of the bulk liquid which needs the bulk liquid direct correlation function  $c^{(2)}(r, \bar{\rho}, T)$  as an input. A functional Taylor expansion around a homogeneous reference density up to second order yields

$$\mathcal{F}_{\text{exc}}(T, [\rho]) \cong -\frac{k_B T}{2} \int d^3 r \int d^3 r' c^{(2)}(|\vec{r} - \vec{r}'|, \bar{\rho}, T) (\rho(\vec{r}) - \bar{\rho})(\rho(\vec{r}') - \bar{\rho}) \quad (12)$$

The RY approximation leads to freezing for hard spheres and was historically the first demonstration that freezing can be described within DFT. The RY functional can readily be generalized to soft interactions [18] (as the OCP) and gives reasonable results for freezing there (though it is better to improve the functional by including triplet correlations).

A non-perturbative functional is based on Rosenfeld's fundamental measure theory (FMT). For more details, see the lectures of R. Evans. This works, however, only for hard spheres. In FMT we have

$$\frac{\mathcal{F}_{\text{exc}}[\rho]}{k_B T} = \int d^3 r \Phi[\{n_\alpha(\vec{r})\}] \quad (13)$$

with

$$n_\alpha(\vec{r}) = \int d^3 r' w^{(\alpha)}(\vec{r} - \vec{r}') \rho(\vec{r}') \quad (14)$$

where the six weight function are given explicitly as

$$w^{(0)}(\vec{r}) = \frac{w^{(2)}(\vec{r})}{\pi\sigma^2} \quad (15)$$

$$w^{(1)}(\vec{r}) = \frac{w^{(2)}(\vec{r})}{2\pi\sigma} \quad (16)$$

$$w^{(2)}(\vec{r}) = \delta\left(\frac{\sigma}{2} - r\right) \quad (17)$$

$$w^{(3)}(\vec{r}) = \Theta\left(\frac{\sigma}{2} - r\right) \quad (18)$$

$$w^{(V_1)}(\vec{r}) = \frac{\vec{w}^{(V_2)}(\vec{r})}{2\pi\sigma} \quad (19)$$

$$w^{(V_2)}(\vec{r}) = \frac{\vec{r}}{r} \delta\left(\frac{\sigma}{2} - r\right) \quad (20)$$

with  $\sigma$  denoting the hard sphere diameter and

$$\Phi = \Phi_1 + \Phi_2 + \Phi_3 \quad (21)$$

$$\Phi_1 = -n_0 \ln(1 - n_3) \quad (22)$$

$$\Phi_2 = \frac{n_1 n_2 - \vec{n}_{v_1} \cdot \vec{n}_{v_2}}{1 - n_3} \quad (23)$$

$$\Phi_3 = \frac{\frac{1}{3}n_2^3 - n_2(\vec{n}_{v_2} \cdot \vec{n}_{v_2})}{8\pi(1 - n_3)^2} \quad (24)$$

This FMT functional yields the Percus-Yevick solution of the direct correlation function as an output. It furthermore survives the dimensional crossover [19]: If the three-dimensional hard sphere system is confined within a one-dimensional tube, the exact Percus functional is recovered. Moreover, in a spheroidal cavity which holds one or no particle at all, the exact functional is recovered. This helps to understand that the constraint packing argument of freezing is geometrically included in the FMT. In fact (also with a tensor modification in  $\Phi_3$  [20]), the FMT gives excellent data for hard-sphere freezing [19], see Table 1.

	$\rho_l \sigma^3$	$\rho_s \sigma^3$	L (: Lindemann)
computer simulations	0.94	1.04	0.129
RY	0.97	1.15	0.06
Rosenfeld	0.94	1.03	0.101

**Table 1:** Coexisting number densities and solid Lindemann parameter at coexistence for the hard sphere systems. "Exact" computer simulation data are shown as well as DFT data using the Ramakrishnan-Youssof (RY) or Rosenfeld's fundamental measure theory.

Last but not least we mention perturbation theories which can be used for attractive tails. The total potential  $V(r)$  is then split into a purely repulsive

short-ranged part  $V_{rep}(r)$  and a longer-ranged attractive part  $V_{attr}(r)$  such that  $V(r) = V_{rep}(r) + V_{attr}(r)$ . The repulsive part is treated as an effective hard core with an effective (temperature-dependent) Barker-Henderson diameter

$$\sigma(T) = \int_0^\infty dr \left(1 - e^{-\beta V_{rep}(r)}\right) \quad (25)$$

and the attractive part is treated within mean-field approximation. Accordingly, the total excess free energy functional reads as

$$\begin{aligned} \mathcal{F}_{exc}(T, [\rho]) &\cong \mathcal{F}_{exc}^{HS}(T, [\rho])|_{\sigma=\sigma(T)} \\ &+ \frac{1}{2} \int d^3r \int d^3r' \rho(\vec{r})\rho(\vec{r}')V_{attr}(|\vec{r}-\vec{r}'|) \end{aligned} \quad (26)$$

This procedure yields good phase diagrams for both Lennard-Jones potentials and sticky-hard-sphere systems including the isostructural solid-solid transition [9].

## Summary

- 1) Rosenfeld's FMT yields excellent data for hard spheres freezing.
- 2) The much less justified RY perturbative approach works in principle for softer repulsions.
- 3) The mean-field density functional approximation works for penetrable potentials.
- 4) Hard sphere perturbation theory yields stability of liquids and solid-solid isostructural transitions.



## 2 Brownian Dynamics and dynamical density functional theory

### 2.1 Brownian dynamics (BD)

Colloidal particles are embedded in a molecular solvent and are therefore randomly kicked by the solvent molecules on timescales much smaller than the drift of the colloidal motion [21][22].

Let us first discuss the Smoluchowski picture. Here the time-dependent density field is the central quantity. It should follow a simple deterministic diffusion equation. For noninteracting particles with an inhomogeneous time-dependent particle density  $\rho(\vec{r}, t)$ , Fick's law states that the current density  $\vec{j}(\vec{r}, t)$  is

$$\vec{j}(\vec{r}, t) = -D\vec{\nabla}\rho(\vec{r}, t) \quad (27)$$

where  $D$  is a phenomenological diffusion coefficient.

The continuity equation of particle conservation

$$\frac{\partial\rho(\vec{r}, t)}{\partial t} + \vec{\nabla} \cdot \vec{j}(\vec{r}, t) = 0 \quad (28)$$

then leads to the wellknown diffusion equation for  $\rho(\vec{r}, t)$ :

$$\frac{\partial\rho(\vec{r}, t)}{\partial t} \equiv D\Delta\rho(\vec{r}, t) \quad (29)$$

In the presence of an external potential  $V_{\text{ext}}(\vec{r})$ , the force  $\vec{F} = -\vec{\nabla}V_{\text{ext}}(\vec{r})$  acts on the particles and will induce a drift velocity  $\vec{v}_{\text{D}}$  resp. an additional current density

$$\vec{j}_{\text{D}} = \rho\vec{v}_{\text{D}}. \quad (30)$$

We now assume totally overdamped motion since inertia effects are small as the colloids are much bigger than the solvent molecules. This results in

$$\vec{v}_{\text{D}} = \frac{\vec{F}}{\xi} = -\frac{1}{\xi}\vec{\nabla}V_{\text{ext}}(\vec{r}) \quad (31)$$

with  $\xi$  denoting a friction coefficient. For a sphere of radius  $R$  in a viscous solvent,  $\xi = 6\pi\eta_s R$ , with  $\eta_s$  denoting the shear viscosity of the solvent (Stokes law). Now the total current density is

$$\vec{j} = -D\vec{\nabla}\rho(\vec{r}, t) - \rho(\vec{r}, t)\frac{1}{\xi}\vec{\nabla}V_{\text{ext}}(\vec{r}) \quad (32)$$

In equilibrium, the one-particle density is a Boltzmann distribution

$$\rho(\vec{r}, t) \equiv \rho^{(1)}(\vec{r}) = \rho^{(0)}(\vec{r}) = A \exp(-\beta V_{\text{ext}}(\vec{r})) \quad (33)$$

Futhermore, in equilibrium, the total current has to vanish, i.e.

$$0 = -D \underbrace{\vec{\nabla}\rho^{(0)}(\vec{r})}_{-\beta A \exp(-\beta V_{\text{ext}}(\vec{r}))\vec{\nabla}V_{\text{ext}}(\vec{r})} - \underbrace{\rho^{(0)}(\vec{r})}_{A \exp(-\beta V_{\text{ext}}(\vec{r}))} \frac{1}{\xi} \vec{\nabla}V_{\text{ext}}(\vec{r}) \quad (34)$$

Therefore, necessarily

$$D = \frac{k_B T}{\xi} \quad (35)$$

which is the so-called Stokes-Einstein relation.

Hence  $\vec{j} = -\frac{1}{\xi}(k_B T \vec{\nabla} \rho + \rho \vec{\nabla} V_{\text{ext}})$   
and the continuity equation yields

$$\frac{\partial \rho(\vec{r}, t)}{\partial t} = \frac{1}{\xi} (k_B T \Delta \rho(\vec{r}, t) + \vec{\nabla}(\rho(\vec{r}, t) \vec{\nabla} V_{\text{ext}}(\vec{r}))) \quad (36)$$

which is called Smoluchowski equation (for non-interacting particles).

The same equation holds for the probability density  $w(\vec{r}, t)$  to find a particle at position  $\vec{r}$  for time  $t$ . For  $N$  non-interacting particles,

$$w(\vec{r}, t) = \frac{1}{N} \rho(\vec{r}, t), \quad (37)$$

and the Smoluchowski equation reads:

$$\frac{\partial w}{\partial t} = \frac{1}{\xi} (k_B T \Delta w - \vec{\nabla}(w \cdot \vec{\nabla} V_{\text{ext}})) \quad (38)$$

Now we consider  $N$  **interacting** particles. Using a compact notation for the particle positions

$$\{x_i\} = \{\vec{r}_i\} = \underbrace{\{x_1, x_2, x_3\}}_{\vec{r}_1}, \underbrace{\{x_4, x_5, x_6, \dots\}}_{\vec{r}_2}, \dots, \underbrace{\{x_{3N-2}, x_{3N-1}, x_{3N}\}}_{\vec{r}_N} \quad (39)$$

we assume a linear relation between acting forces on the particles and the resulting drift velocities. (The same compact notation is used for other multiple vectors.) The details of this relation embody the so-called hydrodynamic interactions mediated between the colloidal particles by the solvent flow field induced by the moving colloidal particles. This linear relation is in general

$$v_i = \sum_{j=1}^{3N} L_{ij}(\{x_n\}) \vec{F}_j \quad (40)$$

where  $\vec{F}_j = -\frac{\partial}{\partial x_j} U_{\text{tot}}$  where  $U_{\text{tot}}$  involves both the internal and the interaction potential energy and  $v$  is the drift velocity. The underlying assumption in (40) is that the hydrodynamic interactions act quasi-instantaneously. This is justified by the fact that the timescale upon which a shear perturbation is traveling through the suspension within an interparticle distance is much smaller than that of Brownian motion. The coefficients  $L_{ij}$  constitute the so-called  $3N \times 3N$  mobility matrix and can in principle be obtained by solving the Navier-Stokes equations of  $N$  spheres with appropriate stick boundary conditions of the solvent flow field on the particle's surfaces.

In general,  $L_{ij}$  depends on  $\vec{r}^N$ , and we postulate:

- symmetry

$$L_{ij} = L_{ji} \quad (41)$$

- positivity

$$\sum_{ij} F_i F_j L_{ij} > 0 \text{ for all } F_{i,j} \neq 0 \quad (42)$$

With  $w(\{\vec{r}_i\}, t)$  denoting the probability density for interacting particles, the suitable generalization of the continuity equation is

$$\frac{\partial w}{\partial t} = - \sum_{n=1}^{3N} \frac{\partial}{\partial x_n} (v_{\text{tot},n} w) \quad (43)$$

with

$$v_{\text{tot},n} = \sum_{m=1}^{3N} L_{mn} \frac{\partial}{\partial x_m} (k_B T \ln w + U_{\text{tot}}) \quad (44)$$

which leads to the generalized Smoluchowski equation for interacting particles.

$$\frac{\partial w}{\partial t} = \hat{\mathcal{O}} w \quad (45)$$

with the Smoluchowski operator

$$\hat{\mathcal{O}} = \sum_{n,m=1}^{3N} \frac{\partial}{\partial x_n} L_{nm} \left( k_B T \frac{\partial}{\partial x_m} + \frac{\partial U_{\text{tot}}}{\partial x_m} \right) \quad (46)$$

In many applications, hydrodynamic interactions are neglected. This means that the mobility matrix is constant and a diagonal

$$L_{nm} = \frac{1}{\xi} \delta_{nm} \quad (47)$$

This assumption, however, is only true for small volume fraction of the colloidal particles.

Complementary to the Smoluchowski approach which considers diffusion in phase space, stochastic trajectories in real-space are the basic ingredients for the Langevin picture. A typical “cuspy” Brownian trajectories of a colloidal particle is shown in Figure 11

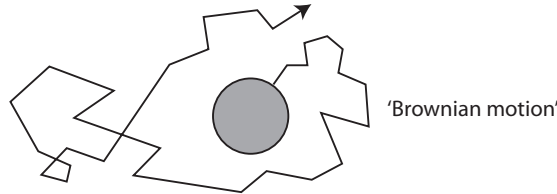


**Figure 11:** Typical trajectory of a randomly kicked Brownian particle.

First, we consider only one particle in an external potential  $V_{\text{ext}}(\vec{r})$  with random force  $\vec{f}(t)$ . The stochastic differential equation for a single particle is completely overdamped

$$\xi \dot{\vec{r}} = -\vec{\nabla} V_{\text{ext}}(\vec{r}) + \vec{f}(t) \quad (48)$$

where  $\vec{f}(t)$  mimicks the random kicks of the solvent and is a Gaussian random variable which fulfills

$$\langle \vec{f}(t) \rangle = 0 \quad (49)$$

$$\langle f_i(t) f_j(t') \rangle = 2\xi k_B T \delta_{ij} \delta(t - t') \quad (50)$$

One can show that this is stochastically equivalent to the Smoluchowski equation of non-interacting particles. Numerical methods to solve these stochastic differential equations are treated in the lectures by A. Ladd.

For interacting particles, the Smoluchowski equation is obtained from the following Langevin equations [21]:

$$\dot{x}_n(t) = \sum_{m=1}^{3N} L_{nm} \left( -\frac{\partial U_{\text{total}}}{\partial x_m} + f_m(t) \right) + k_B T \sum_{m=1}^{3N} \frac{\partial L_{nm}}{\partial x_m} \quad (51)$$

## 2.2 Dynamical density functional theory (DDFT)

Here we derive a deterministic equation for the time-dependent one-particle density from the Smoluchowski equations [17]. We follow the idea of Archer and Evans [23]. First, we recall Smoluchowski equation for the  $N$ -particle density

$$w(\vec{r}_1, \dots, \vec{r}_N, t) \equiv w(\vec{r}^N, t) \quad , \quad \vec{r}^N = \{\vec{r}_1, \dots, \vec{r}_N\} \text{ as}$$

$$\frac{\partial w}{\partial t} = \hat{\mathcal{O}}w = \frac{1}{\xi} \sum_{i=1}^N \vec{\nabla}_i \cdot [k_B T \vec{\nabla}_i + \vec{\nabla}_i U_{\text{tot}}(\vec{r}^N, t)]w \quad (52)$$

with

$$U_{\text{tot}}(\vec{r}^N, t) = \sum_{i=1}^N V_{\text{ext}}(\vec{r}_i, t) + \sum_{\substack{i,j=1 \\ i < j}}^N V(|\vec{r}_i - \vec{r}_j|) \quad (53)$$

Here, hydrodynamic interactions have been neglected. Now the idea is to integrate out degrees of freedom. In fact, an integration yields

$$\rho(\vec{r}_1, t) = N \int d^3 r_2 \dots \int d^3 r_N w(\vec{r}^N, t) \quad (54)$$

The 2-particle density is analogously obtained as

$$\rho^{(2)}(\vec{r}_1, \vec{r}_2, t) = N(N-1) \int d^3 r_3 \dots \int d^3 r_N w(\vec{r}^N, t) \quad (55)$$

Integrating the Smoluchowski equation with  $N \int d^3 r_2 \dots \int d^3 r_N$  yields

$$\begin{aligned} \frac{\partial}{\partial t} \rho(\vec{r}_1, t) = N \cdot \int d^3 r_2 \dots \int d^3 r_N \left\{ \sum_{i=1}^N (k_B T \Delta_i w(\vec{r}^N, t) \right. \\ \left. + \vec{\nabla}_i \left( \vec{\nabla}_i V_{\text{ext}}(\vec{r}_i, t) w(\vec{r}^N, t) \right) \right) \\ \left. + \sum_{\substack{i=1 \\ i < j}}^N \vec{\nabla}_i \left( \vec{\nabla}_i (V(|\vec{r}_i - \vec{r}_j|) w(\vec{r}^N, t)) \right) \right\} \quad (56) \end{aligned}$$

**now:**

$$\begin{aligned} 1) N \int d^3 r_2 \dots \int d^3 r_N \sum_{i=1}^N k_B T \Delta_i w(\vec{r}^N, t) &= k_B T \Delta_1 \rho(\vec{r}_1, t) \\ &+ N \int d^3 r_2 \dots \int d^3 r_N k_B T \sum_{i=2}^N \Delta_i w(\vec{r}^N, t) \quad (57) \end{aligned}$$

$$\begin{aligned} &= k_B T \Delta_1 \rho(\vec{r}_1, t) \\ &+ \sum_{i=2}^N N k_B T \int d^3 r_i \vec{\nabla}_i \underbrace{\left( \vec{\nabla}_i \int d^3 r_2 \dots \int d^3 r_N w(\vec{r}^N, t) \right)}_{\vec{g}(\vec{r}_1, \vec{r}_i, t)} \quad (58) \end{aligned}$$

$$= k_B T \Delta_1 \rho(\vec{r}_1, t) + \sum_{i=2}^N N k_B T \underbrace{\int d^2 \vec{f} \vec{g}(\vec{r}_1, \vec{r}_i, t)}_{=0} \quad (59)$$

since  $w$  decays to zero for large distances.

$$\begin{aligned} 2) N \int d^3 r_2 \dots \int d^3 r_N \sum_{i=1}^N \vec{\nabla}_i (\vec{\nabla}_i V_{\text{ext}}(\vec{r}_i, t) w(\vec{r}^N, t)) \\ = N \int d^3 r_2 \dots \int d^3 r_N \vec{\nabla}_1 (\vec{\nabla}_1 V_{\text{ext}}(\vec{r}_1, t) w(\vec{r}^N, t)) + 0 \quad (60) \end{aligned}$$

$$= \vec{\nabla}_1 ((\vec{\nabla}_1 V_{\text{ext}}(\vec{r}_1, t)) \rho(\vec{r}_1, t)) \quad (61)$$

$$\begin{aligned}
3) \quad & N \int d^3 r_2 \dots \int d^3 r_N \sum_{\substack{i,j=1 \\ i < j}}^N \vec{\nabla}_i \cdot (\vec{\nabla}_i V(|\vec{r}_i - \vec{r}_j|)) w(\vec{r}^N, t) \\
&= N \int d^3 r_2 \dots \int d^3 r_N \vec{\nabla}_1 \cdot \left( \sum_{j=2}^N \vec{\nabla}_1 V(|\vec{r}_1 - \vec{r}_j|) w(\vec{r}^N, t) \right) \quad (62)
\end{aligned}$$

$$\begin{aligned}
& \vec{r}^N \text{ is symmetric in coordinates, set } j = 2 \\
&= N(N-1) \vec{\nabla}_1 \int d^3 r_2 \vec{\nabla}_1 V(|\vec{r}_1 - \vec{r}_2|) \int d^3 r_3 \dots \int d^3 r_N w(\vec{r}^N, t) \quad (63)
\end{aligned}$$

$$= \int d^3 r_2 \vec{\nabla}_1 (\vec{\nabla}_1 V(|\vec{r}_1 - \vec{r}_2|)) \rho^{(2)}(\vec{r}_1, \vec{r}_2, t) \quad (64)$$

Hence in total we get

$$\begin{aligned}
\xi \frac{\partial}{\partial t} \rho(\vec{r}_1, t) &= k_B T \Delta_1 \rho(\vec{r}_1, t) + \vec{\nabla}_1 (\rho(\vec{r}_1, t) \vec{\nabla}_1 V_{\text{ext}}(\vec{r}_1, t)) \\
&+ \vec{\nabla}_1 \int d^3 r_2 \rho^{(2)}(\vec{r}_1, \vec{r}_2, t) \vec{\nabla}_1 V(|\vec{r}_1 - \vec{r}_2|) \quad (65)
\end{aligned}$$

In equilibrium, necessarily  $\frac{\partial \rho(\vec{r}_1, t)}{\partial t} = 0$   
which implies

$$0 = \vec{\nabla} \cdot \left( k_B T \vec{\nabla} \rho(\vec{r}, t) + \rho(\vec{r}, t) \vec{\nabla} V_{\text{ext}}(\vec{r}, t) + \int d^3 r' \rho^{(2)}(\vec{r}, \vec{r}', t) \vec{\nabla} V(|\vec{r} - \vec{r}'|) \right) \quad (66)$$

$$= \vec{\nabla} \cdot \left( k_B T \vec{\nabla} \rho(\vec{r}) + \rho(\vec{r}) \vec{\nabla} V_{\text{ext}}(\vec{r}) + \int d^3 r' \rho^{(2)}(\vec{r}, \vec{r}') \vec{\nabla} V(|\vec{r} - \vec{r}'|) \right) \quad (67)$$

The constant must vanish for  $r \rightarrow \infty$  and is thus identical to zero. Therefore

$$0 = k_B T \vec{\nabla} \rho(\vec{r}) + \rho(\vec{r}) \vec{\nabla} V_{\text{ext}}(\vec{r}) + \int d^3 r' \rho^{(2)}(\vec{r}, \vec{r}') \vec{\nabla} V(|\vec{r} - \vec{r}'|) \quad (68)$$

This is also known as Yvon-Born-Green-hierarchy (YBG).

In equilibrium, DFT implies:

$$\frac{\delta \mathcal{F}}{\delta \rho(\vec{r})} = \mu - V_{\text{ext}}(\vec{r}) \quad (69)$$

$$= k_B T \ln(\Lambda^3 \rho(\vec{r})) + \frac{\delta \mathcal{F}_{\text{exc}}}{\delta \rho(\vec{r})}, \text{ since } \mathcal{F} = \mathcal{F}_{\text{id}} + \mathcal{F}_{\text{exc}} \quad (70)$$

We now apply the gradient which gives:

$$\vec{\nabla} V_{\text{ext}}(\vec{r}) + k_B T \underbrace{\vec{\nabla} \ln(\Lambda^3 \rho(\vec{r}))}_{\frac{1}{\rho(\vec{r})} \vec{\nabla} \rho(\vec{r})} + \vec{\nabla} \frac{\delta \mathcal{F}_{\text{exc}}}{\delta \rho(\vec{r})} = 0 \quad (71)$$

combined with YBG we obtain

$$\int d^3 r' \rho^{(2)}(\vec{r}, \vec{r}') \vec{\nabla} V(|\vec{r} - \vec{r}'|) = \rho(\vec{r}) \vec{\nabla} \cdot \frac{\delta \mathcal{F}_{\text{exc}}[\rho]}{\delta \rho(\vec{r})} \quad (72)$$

We postulate that this argument holds also in nonequilibrium. In doing so, non-equilibrium correlations are approximated by equilibrium ones at the same  $\rho(\vec{r}, t)$  (via a suitable  $V_{\text{ext}}(\vec{r})$  in equilibrium). Equivalently, one can say that it is postulated that pair correlations decay much faster to their equilibrium one than the one-body density. Therefore the basic approximation of DDFT is sometimes called adiabatic approximation. For an alternate approach, see Cichocki and Hess [24].

Hence:

$$\begin{aligned} \xi \frac{\partial \rho(\vec{r}, t)}{\partial t} &= \vec{\nabla} (k_B T \vec{\nabla} \rho(\vec{r}, t) + \rho(\vec{r}, t) \vec{\nabla} V_{\text{ext}}(\vec{r}, t) \\ &\quad + \rho(\vec{r}, t) \vec{\nabla} \frac{\delta \mathcal{F}_{\text{exc}}}{\delta \rho(\vec{r}, t)}) \end{aligned} \quad (73)$$

or equivalently

$$\boxed{\xi \frac{\partial \rho(\vec{r}, t)}{\partial t} = \vec{\nabla} \rho(\vec{r}, t) \vec{\nabla} \frac{\delta \Omega[\rho]}{\delta \rho(\vec{r}, t)}} \quad (74)$$

which constitutes the basic equation of dynamical density functional theory (DDFT).

The applications of DDFT are numerous. The dynamics of a strongly inhomogeneous Brownian fluid has found to be in good agreement with BD computer simulations.

Equation (74) can even be used for a description of crystal growth. If a functional is used which describes freezing, the dynamical evolution of a crystal-like density field can be computed. This was explicitly demonstrated for two-dimensional crystals with dipolar interactions in Ref. [25] by using the RY functional.

### 2.3 Hydrodynamic interactions

How does  $L_{nm}(\{x_j\})$  look like explicitly? Solving the linearized Navier-Stokes equations with the appropriate stick boundary conditions on the particle surfaces, is a difficult problem. Furthermore it is problematic that

- i)  $L_{nm}(\{x_j\})$  is long-ranged in terms of distances between particles
- ii) H.I. have **many-body character**, pair expansion only possible at low concentrations
- iii) H.I. have quite different near-field behaviour. They are divergent lubrication terms.

The linear relationship (40) can be rewritten as

$$\vec{v}_n = \sum_{m=1}^N \bar{\bar{H}}_{nm} \vec{F}_m \quad (75)$$

where each quantity  $\bar{\bar{H}}_{nm}$  is a  $3 \times 3$  matrix. In particular, we can discriminate the following cases:

1) **no H.I.**  $H_{nm} = \mathbb{1} \frac{\delta_{nm}}{\xi}$

2) **Oseen-tensor**

In the Oseen approximation,  $\bar{\bar{H}}_{nn} = \frac{\mathbb{1}}{\xi}$

$$\bar{\bar{H}}_{nm} = \bar{\bar{H}}(\underbrace{\vec{r}_n - \vec{r}_m}_{\vec{r}}) \text{ for } n \neq m \quad (76)$$

with the Oseen tensor

$$\bar{\bar{H}}(\vec{r}) = \frac{1}{8\pi\eta_s} (\mathbb{1} + \hat{r} \otimes \hat{r}) \frac{1}{r}, \quad \hat{r} = \frac{\vec{r}}{r} \quad (77)$$

This is the leading far field term for two particles at large distance  $\vec{r}$ . The symbol  $\otimes$  denotes the dyadic product or tensor product.

3) **Rotne-Prager-tensor**

In this approximation, the next leading correction is included.

$$H_{nn} = \frac{\mathbb{1}}{\xi}, \quad H_{nm} = \bar{\bar{H}}_{RP}(\vec{r}_n - \vec{r}_m) \quad (78)$$

with

$$\bar{\bar{H}}_{RP}(\vec{r}) = \frac{D_0}{k_B T} \left( \frac{3 R_H}{4 r} [\mathbb{1} + \hat{r} \otimes \hat{r}] + \frac{1 R_H^3}{2 r^3} [1 - 3\hat{r} \otimes \hat{r}] \right) \quad (79)$$

Higher order expansions of higher order than  $\frac{1}{r^3}$  are possible. These include also terms of sphere rotation. Finally the triplet contribution can be estimated.



The DDFT can be generalized to hydrodynamic interactions [26]. Again the starting point is the Smoluchowski equation which we now write in the form

$$\frac{\partial w(\vec{r}^N, t)}{\partial t} = \sum_{i,j=1}^N \vec{\nabla}_i \cdot \bar{\bar{H}}_{ij}(\vec{r}^N) \cdot \left[ \vec{\nabla}_j + \vec{\nabla}_j \frac{U_{\text{tot}}(\vec{r}^N, t)}{k_B T} \right] w(\vec{r}^N, t) \quad (80)$$

We use the two particle approximation

$$\bar{\bar{H}}_{ij}(\vec{r}^N) \approx \frac{D_0}{k_B T} \left( \mathbb{1} \delta_{ij} + \delta_{ij} \sum_{i \neq j} \omega_{11}(\vec{r}_i - \vec{r}_e) + (1 - \delta_{ij}) \omega_{12}(\vec{r}_i - \vec{r}_e) \right) \quad (81)$$

on the level of the Rotne-Prager expression

$$\omega_{11}(\vec{r}) = 0 \quad (82)$$

$$\omega_{12}(\vec{r}) = \frac{3}{8} \frac{\sigma_H}{r} (\mathbb{1} + \hat{r} \otimes \hat{r}) + \frac{1}{16} \left( \frac{\sigma_H}{r} \right)^3 (1 - 3\hat{r} \otimes \hat{r}) + O\left(\left(\frac{\sigma_H}{r}\right)^7\right) \quad (83)$$

where  $\sigma_H$  is the hydrodynamic diameter.

Integrating Smoluchowski equation [17] then yields [26]

$$\begin{aligned} \frac{k_B T}{D_0} \frac{\partial \rho(\vec{r}, t)}{\partial t} = \nabla_r \cdot & \left[ \rho(\vec{r}, t) \nabla_r \frac{\delta \mathcal{F}[\rho]}{\delta \rho(\vec{r}, t)} \right. \\ & + \int d\vec{r}' \rho^{(2)}(\vec{r}, \vec{r}', t) \omega_{11}(\vec{r} - \vec{r}') \cdot \nabla_r \frac{\delta \mathcal{F}[\rho]}{\delta \rho(\vec{r}, t)} \\ & \left. + \int d\vec{r}' \rho^{(2)}(\vec{r}, \vec{r}', t) \omega_{12}(\vec{r} - \vec{r}') \cdot \nabla_r \frac{\delta \mathcal{F}[\rho]}{\delta \rho(\vec{r}, t)} \right] \quad (84) \end{aligned}$$

A possible closure is via the Ornstein-Zernike equation

$$\begin{aligned} \rho^{(2)}(\vec{r}, \vec{r}', t) = (1 + c^{(2)}(\vec{r}, \vec{r}')) \rho(\vec{r}, t) \rho(\vec{r}', t) \\ + \rho(\vec{r}', t) \int d\vec{r}'' ((\rho^{(2)}(\vec{r}, \vec{r}'', t) - \rho(\vec{r}, t) \rho(\vec{r}'', t)) c^{(2)}(\vec{r}'', \vec{r}')) \quad (85) \end{aligned}$$

with

$$c^{(2)}(\vec{r}, \vec{r}') = -\beta \frac{\delta^2 \mathcal{F}_{\text{exc}}[\rho]}{\delta \rho(\vec{r}, t) \delta \rho(\vec{r}', t)} \quad (86)$$

In an easier attempt, one can approximate

$$\rho^{(2)}(\vec{r}, \vec{r}', t) \approx \rho(r, t) \rho(r', t) g(|\vec{r} - \vec{r}'|, \bar{\rho}) \quad (87)$$

where  $\bar{\rho}$  is a suitable averaged density and  $g(r, \bar{\rho})$  is a pair distribution function in the equilibrium bulk fluid.

Good agreement was obtained between DDFT and BD computer simulations [27] for colloids in unstable traps [26].

## 3 Density functional theory for rod-like particles

### 3.1 Statistical mechanics of rod-like particles

Density functional theory can readily be extended to rod-like particles which possess an additional orientational degree of freedom described by a unit vector  $\hat{u}$ . A configuration of  $N$  particles is now fully specified by the set of positions of the center of masses and the corresponding orientations  $\{\vec{R}_i, \hat{u}_i, i = 1, \dots, N\}$ , see Figure 12.

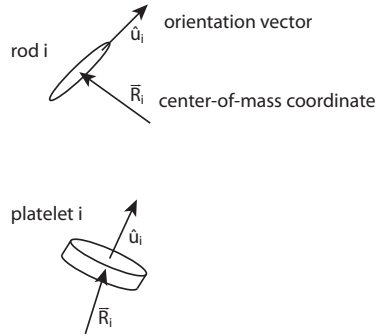


**Figure 12:** Sketch of the center-of-mass position  $\vec{R}_i$  and the orientational unit vector  $\hat{u}_i$  for the  $i^{\text{th}}$  particle both for a rod-like and plate-like particle.

Example for anisotropic particles include

- (1) molecular dipolar fluids (e.g.  $\text{H}_2\text{O}$  molecule)
- (2) rod-like colloids (e.g. tobacco-mosaic viruses)
- (3) molecular fluids without dipole moment (apolar), (e.g.  $\text{H}_2$  molecule)
- (4) plate-like objects (clays)

The canonical partition function for rod-like particles now reads [28]

$$\begin{aligned}
 Z = & \frac{1}{h^{6N} N!} \int_V d^3 R_1 \dots \int_V d^3 R_N \int_{\mathbb{R}^3} d^3 p_1 \dots \int_{\mathbb{R}^3} d^3 p_N \\
 & \times \int_{S_2} d^2 u_1 \dots \int_{S_2} d^2 u_N \int_{\mathbb{R}^3} d^3 L_1 \dots \int_{\mathbb{R}^3} d^3 L_N e^{-\beta \mathcal{H}} \quad (88)
 \end{aligned}$$

with the Hamilton function

$$\begin{aligned}
 \mathcal{H} = & \sum_{i=1}^N \left\{ \frac{\vec{p}_i^2}{2m} + \frac{1}{2} \vec{L}_i (\bar{\Theta})^{-1} \vec{L}_i \right\} + \frac{1}{2} \sum_{i,j=1}^N v(\vec{R}_i - \vec{R}_j, \hat{u}_i, \hat{u}_j) \\
 & + \sum_{i=1}^N V_{\text{ext}}(\vec{R}_i, \hat{u}_i) \quad (89)
 \end{aligned}$$

which comprises the kinetic energy, the pair interaction energy and the external energy. Here  $\bar{\Theta}$  is the inertia tensor and  $S_2$  the unit-sphere in 3d.

Again the central quantity is the one-particle density  $\rho_0^{(1)}(\vec{r}, \hat{u})$  which is defined as

$$\rho_0^{(1)}(\vec{r}, \hat{u}) := \left\langle \sum_{i=1}^N \delta(\vec{r} - \vec{R}_i) \delta(\hat{u} - \hat{u}_i) \right\rangle \quad (90)$$

Integrating the orientations over the unit sphere  $S_2$  results in the density of the center-of-masses

$$\rho_0(\vec{r}) = \frac{1}{4\pi} \int_{S_2} d^2u \rho_0^{(1)}(\vec{r}, \hat{u}) \quad (91)$$

On the other hand, the globally averaged orientational order is gained by integrating over the center-of-mass coordinates and given by

$$f(\hat{u}) = \frac{1}{V} \int_V d^3r \rho_0^{(1)}(\vec{r}, \hat{u}) \quad (92)$$

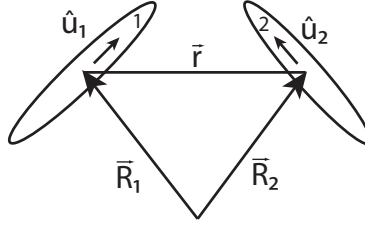


**Figure 13:** Sketch of two interacting rods. The interaction potential depends on  $\vec{r} = \vec{R}_1 - \vec{R}_2$  and  $\hat{u}_1, \hat{u}_2$ .

In analogy to the isotropic case, one can define a pair correlation function

$$g(\vec{R}_1, \vec{R}_2, \hat{u}_1, \hat{u}_2) := \frac{\left\langle \sum_{\substack{i,j=1 \\ i \neq j}}^N \delta(\vec{R}_1 - \vec{R}_i) \delta(\vec{R}_2 - \vec{R}_j) \delta(\hat{u}_1 - \hat{u}_i) \delta(\hat{u}_2 - \hat{u}_j) \right\rangle}{\rho_0^{(1)}(\vec{R}_1, \hat{u}_1) \rho_0^{(1)}(\vec{R}_2, \hat{u}_2)} \quad (93)$$

Now different phases are conceivable which can be classified and distinguished by their one-particle density field.

#### 1) fluid (disordered) phase, isotropic phase

Here the center-of-mass-positions and orientations are disordered, see Figure 14:

$$\rho_0^{(1)}(\vec{r}, \hat{u}) = \rho_0 = \text{const} \quad (94)$$

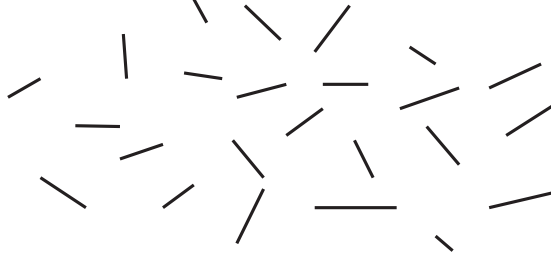


**Figure 14:** Sketch of a typical particle configuration in the isotropic phase.

2) nematic phase

Here, positions are disordered and orientations are ordered, i.e.

$$\rho_0^{(1)}(\vec{r}, \hat{u}) = \rho f(\hat{u}) \quad , \quad \hat{u}_0 : \text{nematic director} \quad (95)$$

Typically the orientation is distributed around a nematic director  $\hat{u}_0$ , see Figure 15.

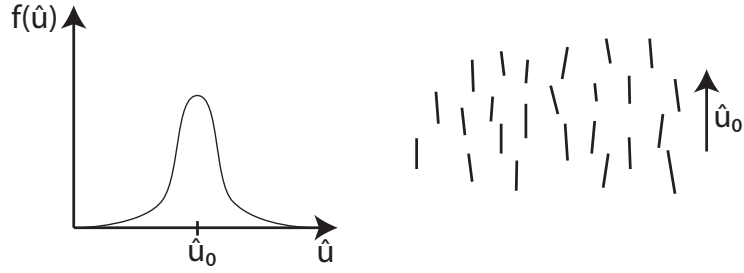


**Figure 15:** Left: Orientational distribution in the nematic phase (schematic). Right: Typical particle configuration in the nematic phase with a nematic director  $\hat{u}_0$ .

In order to quantify orientational order, it is convenient to introduce a nematic order parameter. In fact, this is defined via the second rank tensor

$$\bar{\bar{Q}} = \left\langle \frac{1}{N} \sum_{i=1}^N \left( \frac{3}{2} \hat{u}_i \otimes \hat{u}_i - \frac{1}{2} \mathbb{1} \right) \right\rangle \quad (96)$$

where the dyadic product is

$$\hat{u}_i \otimes \hat{u}_i = \begin{pmatrix} u_{ix}u_{ix} & u_{ix}u_{iy} & u_{ix}u_{iz} \\ u_{iy}u_{ix} & u_{iy}u_{iy} & u_{iy}u_{iz} \\ u_{iz}u_{ix} & u_{iz}u_{iy} & u_{iz}u_{iz} \end{pmatrix} \quad (97)$$

One can easily show that the tensor  $\bar{\bar{Q}}$  is trace-less

$$\text{Tr} \bar{\bar{Q}} = \frac{1}{2} \langle \text{Tr}(3\hat{u}_i \otimes \hat{u}_i - \mathbb{1}) \rangle \quad (98)$$

$$= \frac{1}{2} \langle 3 \cdot 1 - 3 \rangle = 0 \quad (99)$$

Furthermore  $\bar{Q}$  is clearly symmetric and hence diagonalizable with three eigenvalues  $\lambda_1 \geq \lambda_2 \geq \lambda_3$  where  $\lambda_3$  must be  $-\lambda_2 - \lambda_1$ . The largest eigenvalue  $\lambda_1$  is called nematic order parameter  $S$ . The corresponding eigenvector is called nematic director. For perfect alignment along  $\vec{u}_0$  we have  $\vec{u}_i \equiv \hat{u}_0$  for all  $i$ . Then,  $S = 1$ . If the two lower eigenvalues are identical,  $\lambda_2 = \lambda_3$ , we call it a **uniaxial nematic** phase. If  $\lambda_2 \neq \lambda_3$ , the orientation is called **biaxial**. In the **isotropic phase**:  $S = 0$ . Orientational distributions are accessible experimentally, by e.g. birefringence.

### 3) smectic-A phase

The so-called smectic-A phase is positionally ordered along an orientation axis  $\hat{u}_0$ , see Figure 16. The associated one-particle density is periodic in the  $z$ -direction along  $\hat{u}_0$ :

$$\rho_0^{(1)}(\vec{r}, \hat{u}) = \rho(z, \hat{u}) \quad z\text{-periodic} \quad (100)$$

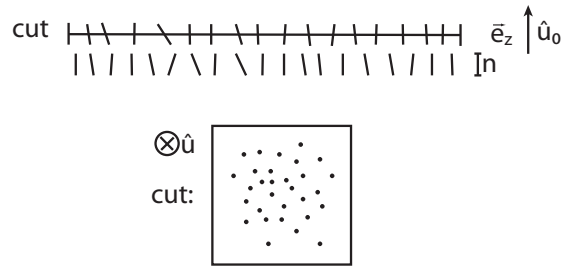


**Figure 16:** Typical particle configuration in the smectic-A phase in the plane of  $\hat{u}_0$  and perpendicular to  $\hat{u}_0$ .

### 4) smectic-B phase

The smectic-B phase is similar to the smectic-A phase but exhibits an in-plane triangular lattice as indicated in Figure 17.

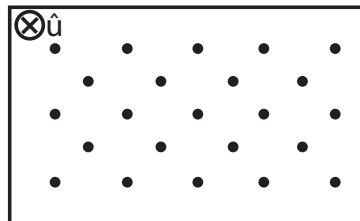


**Figure 17:** Typical particle configuration in the smectic-B phase perpendicular to  $\hat{u}_0$ .

5) columnar phase

The columnar exhibits crystalline order perpendicular to the director  $\hat{u}_0$  but is disordered positionally along  $\vec{u}_0$ . The one-particle density field thus reads as

$$\rho_0^{(1)}(\vec{r}, \hat{u}) = \rho(x, y, \hat{u}) \quad (101)$$

6) plastic crystal

In a plastic crystal, the positions are ordered in all three spatial directions but the orientations are disordered, see Figure 18. Therefore:

$$\rho_0^{(1)}(\vec{r}, \hat{u}) = f(\vec{r}) \quad (102)$$

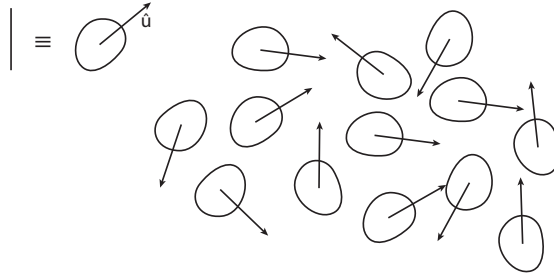


**Figure 18:** Snapshot of a plastic crystal.

7) full crystalline phases

Finally, in the full crystalline phase, positions and orientations are both ordered, see Figure 19.

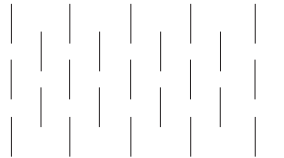


**Figure 19:** Snapshot of a full crystalline phase.

The list (1)-(7) of liquid crystalline phases is by far not exhaustive. There are more “exotic” phases such as an AAA stacked phase, a smectic-C with tilted rods, or cholesteric phases which possesses a helical twist with a pitch length  $l_p$ , see Figure 20.

### 3.2 Simple models

Let us now discuss simple models for interactions between anisotropic rods. The phase behaviour of hard objects, as shown in Figure 21, is dominated by the shape. Temperature scales out in this case such that packing fraction alone (apart from the particle shape) is the only parameter. Hard spherocylinders

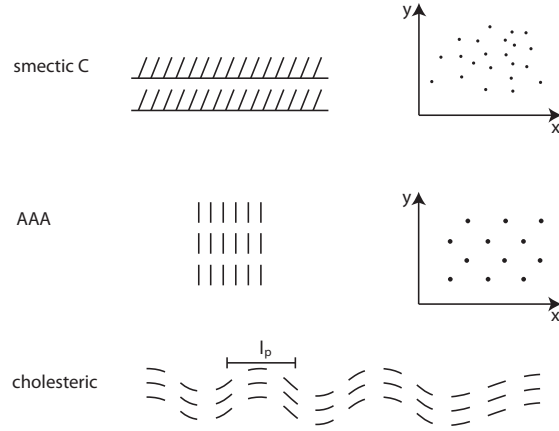


**Figure 20:** Typical particle configurations of the AAA-phase, the smectic-C and the cholesteric phase.

have been studied, as well as hard platelets (“hard coins”) or thin needles which arise from spherocylinders in the limit of infinite aspect ratio  $\frac{L}{D} \rightarrow \infty$ .



**Figure 21:** Sketch of differently shaped hard bodies.

A) Analytical results by Onsager

In the limit  $p = \frac{L}{D} \rightarrow \infty$ , a virial expansion up to second order is getting asymptotically exact. There is a isotropic-nematic transition which can be calculated analytically [29]. It is first order with a density jump. The scaled coexistence densities of the coexisting isotropic and nematic phases are

$$\rho_{\text{iso}} L^2 D = 4.189 \dots \quad (103)$$

and

$$\rho_{\text{nem}} L^2 D = 5.376 \dots \quad (104)$$

At coexistence, the nematic order parameter in the nematic phase is  $S = 0.784$ . The phase diagram is shown qualitatively in Figure 22. However, in practice, one needs pretty large aspect ratios (about  $p \gtrsim 200$ ) in order to get reasonably into this Onsager limit.

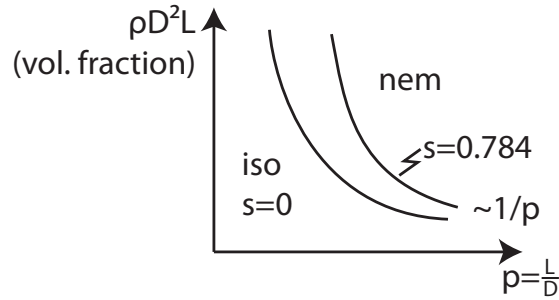


**Figure 22:** Isotropic-nematic phase diagram in the plane of reduced particle number density  $\rho D^2 L$  and as aspect ratio  $p = \frac{L}{D}$ , the density jump is also included.

### B) Computer simulations

Full phase diagrams can be obtained by Monte Carlo computer simulations [30]. Hard spherocylinders show for various densities  $\rho$  and aspect ratios  $p$  the following stable phases as sketched in Figure 23: isotropic, plastic, ABC stacking, AAA stacking, smectic-A, and nematic phases. All those transitions are purely driven by entropy.

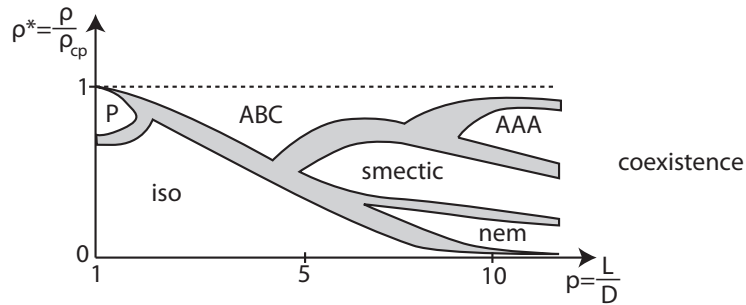


**Figure 23:** Topology of the bulk phase diagram for hard spherocylinders. The density  $\rho$  is scaled in terms of its close-packed density  $\rho_{cp}$  which corresponds to an ABC stacked crystal. The following phases have a stable region in the plane spanned by density and aspect ratio  $p$ : isotropic (iso), nematic (nem), plastic crystal (P), ABC-stacked crystal (ABC), smectic-A phase (smectic), AAA-stacked crystal (AAA). The grey zones indicate coexistence regions

Another anisotropic system are hard ellipsoids which are characterized by two different axial lengths  $a$  and  $b$  as shown in Figure 24. The phase diagram, as sketched in Figure 24 involves isotropic, nematic fully crystalline and plastic crystalline phases [31]. There is a remarkable symmetry in  $x \rightarrow \frac{1}{x}$  for the topology of the phase diagram where  $x = \frac{a}{b}$ .  $x < 1$  correspond to oblate and  $x > 1$  to prolate objects.



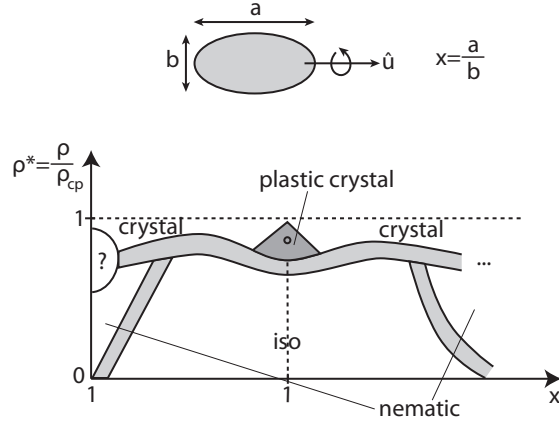


**Figure 24:** Phase diagram of hard ellipsoids versus  $x = \frac{a}{b}$  with a similar notation as in Figure 23.

### C) Density functional theory

Again density functional theory tells us that there exists a unique grandcanonical free energy functional  $\Omega(T, \mu, [\rho^{(1)}])$  (functional of the one-particle density) which becomes minimal for the equilibrium density  $\rho_0^{(1)}(\vec{r}, \hat{u})$  and then equals the real grand canonical free energy, i.e.

$$\left. \frac{\delta \Omega(T, \mu, [\rho^{(1)}])}{\delta \rho^{(1)}(\vec{r}, \hat{u})} \right|_{\rho^{(1)} = \rho_0^{(1)}(\vec{r}, \hat{u})} = 0 \quad (105)$$

Here, the functional can be decomposed as follows

$$\begin{aligned} \Omega(T, \mu, [\rho^{(1)}]) &= k_B T \int d^3 r \int d^2 u \rho^{(1)}(\vec{r}, \hat{u}) [\ln(\Lambda^3 \rho^{(1)}(\vec{r}, \hat{u})) - 1] \\ &+ \int d^3 r d^2 u (V_{\text{ext}}(\vec{r}, \hat{u}) - \mu) \rho^{(1)}(\vec{r}, \hat{u}) + \mathcal{F}_{\text{exc}}(T, [\rho^{(1)}]) \quad (106) \end{aligned}$$

The first term on the right hand side of equation (106) is the functional  $\mathcal{F}_{\text{id}}[\rho^{(1)}]$  for ideal rotators. The excess part  $\mathcal{F}_{\text{exc}}(T, [\rho^{(1)}])$  is in general unknown and requires approximative treatments.

For hard spherocylinders,  $\mathcal{F}_{\text{exc}}(T, [\rho^{(1)}])$  can be approximated by a smoothed density approximation (SMA) [32] yielding several stable liquid-crystalline phases, namely: isotropic, nematic, smectic-A and ABC crystalline. A modified weighted density approximation (MWDA) was subsequently proposed [33] which improves upon the SMA by exhibiting stable plastic crystalline and AAA crystals as well. An important recent progress was achieved by generalizing Rosenfeld's fundamental measure theory from hard spheres to hard objects with any shape [34]. For spherocylinders the functional was worked out explicitly. This functional could be exploited also for attractions by employing a perturbation theory for

the attractive parts in the potential. Finally, a mean-field density functional for rods with soft segments was proposed and studied [35].

### 3.3 Brownian dynamics of rod-like particles

In order to derive a dynamical density functional theory (DDFT) for rod-like particles one can start from the Smoluchowski equation for the full probability density distribution  $w(\vec{r}_1, \dots, \vec{r}_N; \vec{u}_1, \dots, \vec{u}_N, t)$  of  $N$  rods with their corresponding center-of-mass positions  $\vec{r}^N = (\vec{r}_1, \dots, \vec{r}_N)$  and orientations  $\hat{u}^N = (\hat{u}_1, \dots, \hat{u}_N)$  which reads [36]

$$\frac{\partial w}{\partial t} = \hat{\mathcal{O}}_S w \quad (107)$$

where the Smoluchowski operator is now given by

$$\begin{aligned} \hat{\mathcal{O}}_S = \sum_{i=1}^N \left[ \vec{\nabla}_{\vec{r}_i} \cdot \bar{\bar{D}}(\hat{u}_i) \cdot \left( \vec{\nabla}_{\vec{r}_i} + \frac{1}{k_B T} \vec{\nabla}_{\vec{r}_i} U(\vec{r}^N, \hat{u}^N, t) \right) \right. \\ \left. + D_r \hat{R}_i \cdot \left( \hat{R}_i + \frac{1}{k_B T} \hat{R}_i U(\vec{r}^N, \hat{u}^N, t) \right) \right] \end{aligned} \quad (108)$$

where  $U(\vec{r}^N, \hat{u}^N, t)$  is the total potential energy. Here the rotation Operator  $\hat{R}_i$  is defined as  $\hat{R}_i = \hat{u}_i \times \vec{\nabla}_{\hat{u}_i}$  and the anisotropic translational diffusion tensor is given by

$$\bar{\bar{D}}(\hat{u}_i) = D^{\parallel} \hat{u}_i \otimes \hat{u}_i + D^{\perp} (\mathbb{1} - \hat{u}_i \otimes \hat{u}_i) \quad (109)$$

The two diffusion constants  $D^{\parallel}$  and  $D^{\perp}$ , parallel and perpendicular to the orientations reflect the fact that the translational diffusion is anisotropic. For hard spherocylinders there are valid approximations for  $D^{\parallel}$  and  $D^{\perp}$  [37].

Following the idea of Archer and Evans [23] one can integrate the Smoluchowski equation by now applying  $N \int d^3 r_2 \dots \int d^3 r_N \int d^2 u_1 \dots \int d^2 u_n$  on both sides of Eqn (107). This results in [35]:

$$\begin{aligned} \frac{\partial \rho(\vec{r}, \hat{u}, t)}{\partial t} = \vec{\nabla}_{\vec{r}} \cdot \bar{\bar{D}}(\hat{u}) \cdot \left[ \vec{\nabla}_{\vec{r}} \rho(\vec{r}, \hat{u}, t) + \frac{1}{k_B T} \rho(\vec{r}, \hat{u}, t) \cdot \vec{\nabla}_{\vec{r}} V_{\text{ext}}(\vec{r}, \hat{u}, t) - \frac{\vec{F}(\vec{r}, \hat{u}, t)}{k_B T} \right] \\ + D_r \hat{R} \cdot \left[ \hat{R} \rho(\vec{r}, \hat{u}, t) + \frac{1}{k_B T} \rho(\vec{r}, \hat{u}, t) \vec{\nabla}_{\vec{r}} V_{\text{ext}}(\vec{r}, \hat{u}, t) - \frac{1}{k_B T} \vec{T}(\vec{r}, \hat{u}, t) \right] \end{aligned} \quad (110)$$

with an average force

$$\vec{F}(\vec{r}, \hat{u}, t) = - \int d^3 r' \int d^2 u' \rho^{(2)}(\vec{r}, \vec{r}', \hat{u}, \hat{u}', t) \vec{\nabla}_{\vec{r}} v_2(\vec{r} - \vec{r}', \hat{u}, \hat{u}') \quad (111)$$

and average torque

$$\vec{T}(\vec{r}, \hat{u}, t) = - \int d^3 r' \int d^2 u' \rho^{(2)}(\vec{r}, \vec{r}', \hat{u}, \hat{u}', t) \hat{R} v_2(\vec{r} - \vec{r}', \hat{u}, \hat{u}') \quad (112)$$

The two-particle density which is in general unknown can be approximated in equilibrium by using

$$\vec{F}(\vec{r}, \hat{u}, t) = \rho_0(\vec{r}, \hat{u}) \vec{\nabla}_{\vec{r}} \frac{\delta \mathcal{F}_{\text{exc}}(T, [\rho_0])}{\delta \rho_0(\vec{r}, \hat{u})} \quad (113)$$

respectively

$$\vec{T}(\vec{r}, \hat{u}, t) = \rho_0(\vec{r}, \hat{u}) \hat{R} \frac{\delta \mathcal{F}_{\text{exc}}[\rho]}{\delta \rho_0(\vec{r}, \hat{u})} \quad (114)$$

Similar as in the isotropic (spherical) case we now employ the “adiabatic” approximation. We assume that the pair correlations in nonequilibrium are the same as those for an equilibrium system with the same one-body density profile (established by a suitable  $V_{\text{ext}}(\vec{r}, \hat{u}, t)$ ). The resulting dynamical equation for the time-dependent one particle density  $\rho(\vec{r}, \hat{u}, t)$  is then given by Ref. [35].

$$\begin{aligned} \frac{\partial \rho(\vec{r}, \hat{u}, t)}{\partial t} = & \vec{\nabla}_{\vec{r}} \cdot \bar{D}(\hat{u}) \cdot \left[ \rho(\vec{r}, \hat{u}, t) \vec{\nabla}_{\vec{r}} \frac{\delta \mathcal{F}[\rho(\vec{r}, \hat{u}, t)]}{\delta \rho(\vec{r}, \hat{u}, t)} \right] \\ & + D_r \hat{R} \left[ \rho(\vec{r}, \hat{u}, t) \hat{R} \frac{\delta \mathcal{F}[\rho(\vec{r}, \hat{u}, t)]}{\delta \rho(\vec{r}, \hat{u}, t)} \right] \end{aligned} \quad (115)$$

with the equilibrium Helmholtz free energy density functional

$$\begin{aligned} \mathcal{F}[\rho] = & k_B T \int d^3 r \int d\hat{u} \rho(\vec{r}, \hat{u}) [\ln(\Lambda^3 \rho(\vec{r}, \hat{u})) - 1] \\ & + \mathcal{F}_{\text{exc}}(T, [\rho]) + \int d^3 r \int d\hat{u} \rho(\vec{r}, \hat{u}) V_{\text{ext}}(\vec{r}, \hat{u}, t) \end{aligned} \quad (116)$$

This sets the frame for dynamical density functional theory (DDFT) for rods.

As for a special application of DDFT to dynamics in the confined isotropic phase we refer to [35] where the mean-field approximation for the functional was employed. More recent work has used the Rosenfeld functional for hard spherocylinders [34] for driven nematic phases [38].

Finally, DDFT was also applied to self-propelled rods in order to predict the collective swarming and clustering behavior of “active” rods in confinement [39].

## 4 Conclusions

In conclusion, density functional theory provides an excellent statistical mechanical framework and a versatile tool for equilibrium and nonequilibrium situations. This was shown explicitly for the freezing transition of spherical-symmetric pair potentials and for rod-like systems. For Brownian dynamics, density functional theory can be made time-dependent in order to tackle various nonequilibrium phenomena.

**Acknowledgement:** I thank R. Evans, M. Rex, H. H. Wensink, S. van Teeffelen and A. Härtel for many helpful suggestions and T. Glanz, M. Kohl and B. Schumann for support in typing this manuscript. This work was supported by the DFG (SPP1296 and SFB TR6 (project D3)).

## References

- [1] R. Evans, *Advances in Physics* **28**, 143 (1979).
- [2] D. W. Oxtoby, in: *Liquids, Freezing and Glass Transition*, edited by J. P. Hansen, D. Levesque, J. Zinn-Justin, North Holland, Amsterdam, pages 145-189, 1991.
- [3] H. Löwen, *Physics Reports* **237**, 249 (1994).
- [4] J.-L. Barrat, J.-P. Hansen, *Basic Concepts for Simple and Complex Liquids*, Cambridge University Press, 2003.
- [5] H. Löwen, *J. Phys.: Condensed Matter* **14**, 11897 (2002).
- [6] P. Tarazona, J. A. Cuesta, Y. Martinez-Raton, *Density functional Theories of Hard Particle Systems*, *Lect. Notes Phys.* **753**, Springer, Berlin, pages 247-341 (2008).
- [7] J. P. Hansen, I. McDonald, *Theory of Simple Liquids*. 3rd Edition, Elsevier, Amsterdam, Academic Press 2005.
- [8] M. P. Allen, D. J. Tildesley, *Computer Simulation of Liquids*, Oxford Science Publications, Clarendon Press, Oxford, 1987.
- [9] C. N. Likos, Z. T. Németh, H. Löwen, *J. Phys.: Condensed Matter* **6**, 10965 (1994).
- [10] C. N. Likos, H. Löwen, M. Watzlawek, B. Abbas, O. Jucknischke, J. Allgaier, D. Richter, *Phys. Rev. Letters* **80**, 4450 (1998).
- [11] M. Watzlawek, C. N. Likos, H. Löwen, *Phys. Rev. Letters*. **82**, 5289 (1999).
- [12] A. Lang, C. N. Likos, M. Watzlawek, H. Löwen, *J. Phys.: Condensed Matter* **12**, 5087 (2000).
- [13] D. Gottwald, C. N. Likos, G. Kahl, H. Löwen, *Phys. Rev. Letters* **92**, 068301 (2004).
- [14] C. N. Likos, A. Lang, M. Watzlawek, H. Löwen, *Phys. Rev. E* **63**, 031206 (2001).
- [15] R. Evans, lecture notes of this summer school.
- [16] R. Ohnesorge, H. Löwen, H. Wagner, *Europhys. Letters* **22**, 245 (1993).
- [17] A. J. Archer, *Phys. Rev. E* **72**, 051501 (2005).
- [18] S. van Teeffelen, N. Hoffmann, C. N. Likos, H. Löwen, *Europhysics Letters* **75**, 583 (2006).
- [19] Y. Rosenfeld, M. Schmidt, H. Löwen, P. Tarazona, *Phys. Rev. E* **55**, 4245 (1997).
- [20] P. Tarazona. *Phys. Rev. Letters* **84**, 694 (2000).

- [21] M. Doi, S. F. Edwards, *The Theory of Polymer Dynamics*, Oxford Science Publications, Clarendon Press Oxford (1986).
- [22] P. N. Pusey, in: *Liquids, Freezing and Glass Transition*, edited by J. P. Hansen, D. Levesque, J. Zinn-Justin, North Holland, Amsterdam, pages 145-189, 1991.
- [23] A. J. Archer, R. Evans, *J. Chem. Phys.* **121**, 4246 (2004).
- [24] B. Cichocki, W. Hess, *Physica A* **141**, 475 (1987).
- [25] S. van Teeffelen, C. N. Likos, H. Löwen, *Phys. Rev. Letters* **100**, 108302 (2008).
- [26] M. Rex, H. Löwen, *Phys. Rev. Letters* **101**, 148302 (2008).
- [27] H. Löwen, *J. Phys.: Condensed Matter* **20**, 404201 (2008).
- [28] D. Frenkel, in: *Liquids, Freezing and Glass Transition*, edited by J. P. Hansen, D. Levesque, J. Zinn-Justin, North Holland, Amsterdam, pages 689-756, 1991.
- [29] L. Onsager, *Proc. New York Acad. Sci.* **51**, 627 (1949).
- [30] P. Bolhuis, D. Frenkel, *J. Chem. Phys.* **106**, 666 (1997).
- [31] D. Frenkel, B. M. Mulder, J. P. McTague, *Phys. Rev. Letters* **52**, 287 (1984).
- [32] A. Poniewierski, R. Holyst, *Phys. Rev. Letters* **61**, 2461 (1988).
- [33] H. Graf, H. Löwen, *J. Phys.: Condensed Matter*, **11**, 1435 (1999).
- [34] H. Hansen-Goos, K. Mecke, *Phys. Rev. Letters* **102**, 018302 (2009).
- [35] M. Rex, H. H. Wensink, H. Löwen, *Phys. Rev. E* **76**, 021403 (2007).
- [36] J. K. G. Dhont, *An Introduction to Dynamics of Colloids*, Elsevier, Amsterdam, 1996.
- [37] H. Löwen, *Phys. Rev. E* **50**, 1232 (1994).
- [38] A. Härtel, H. Löwen, to be published.
- [39] H. H. Wensink, H. Löwen, *Phys. Rev. E* **78**, 031409 (2008).